Theoretical description of spin-resolved appearance potential spectroscopy

H. Ebert and V. Popescu
Institute for Physical Chemistry, University of Munich, Theresienstrasse 37, D-80333 München, Germany
(Received 28 May 1997)

A theoretical description of spin-resolved appearance potential spectroscopy is presented on the basis of a single-particle description of the underlying electronic structure. The final expression for the signal intensity turns out to be essentially a cross-section-weighted self-convolution of the density of states above the Fermi energy, in close analogy to the result for core-valence-valence Auger electron spectroscopy. Application of the formalism presented to bcc Fe and fcc Ni leads to results in very satisfying agreement with corresponding experimental data. Because this is achieved only by treating the involved transition matrix elements in a proper way, their properties are discussed in some detail. [S0163-1829(97)03344-4]

I. INTRODUCTION

Appearance potential spectroscopy (APS) was developed about two decades ago by Houston and Park.[1–3] Since then, it was successfully used as a component selective probe for unoccupied electronic states in solids and at surfaces.[4,5] Simply spoken, APS is an inverse Auger electron spectroscopy (AES) experiment; i.e., one records the rate of core hole creation, using either emitted fluorescence radiation or Auger electrons, as a function of the energy of a primary incoming electron beam. Accordingly, APS turned out to be especially suited to study surface-specific problems such as adsorbate systems.[6,7] Kirschner extended the application of APS to the study of magnetic systems by using a spin-polarized primary electron beam.[8] His experiment on Fe was later refined by Dose and co-workers and extended to other bulk materials[9,10] as well as surface systems.[11]

For the counterpart of APS, the CVV core-valence-valence (CVV) AES, it was recognized quite early that the corresponding signal intensity primarily supplies a measure for the self-convolution of the density of states (DOS) below the Fermi energy E_F.[12] In analogy, APS is in general assumed to map this quantity for unoccupied states above E_F.[9] This interpretation triggered the development of deconvolution techniques meant to derive DOS curves from experimental APS spectra that can be compared to corresponding theoretical curves obtained from band-structure calculations.[13,14] However, a more satisfying and unambiguous way to discuss APS spectra is to calculate them directly starting from a proper description of the underlying electronic structure. In recent years several such theoretical schemes have been developed by various groups,[15–18] emphasizing again the close relationship of CVV AES and APS. Nearly all of the former theoretical investigations stress the importance of many body or correlation effects for the APS spectra (see in particular the overview given in Ref. 18). In particular, the conditions for which satellites may split off from the essentially bandlike basic spectrum has been investigated by Nolting and co-workers.[15–17]

In the following, an alternative theoretical approach to deal with spin-resolved APS spectra of magnetic materials will be presented. It consists essentially in an appropriate extension of the description of CVV AES developed by Hörmandinger *et al.*[19] Within the approach to be described all exchange and correlation effects are treated in an effective way within the framework of local spin-density-functional theory that is used as a basis to calculate the underlying electronic structure. In contrast to the previous theoretical description of APS, more emphasis is laid here on the details of the band structure and the involved matrix elements. As it will be demonstrated below, satisfying agreement can be achieved that way with spin-resolved experimental spectra for Fe and Ni, which obviously show no correlation-induced satellites.

II. EXPRESSION FOR THE APS SIGNAL INTENSITY

In deriving an expression for the APS signal intensity all relativistic effects will be ignored in the following. This means in particular that the spin-orbit splitting for the core states involved will not be accounted for. In addition, it will be assumed that the signal is exclusively determined by the central APS transition, i.e., the detection mode, e.g., fluorescence yield or Auger electron current, has no influence on its intensity and energy dependence. With these assumptions one can start from the standard expression for the Auger process transition probability[20]

$$P=\frac{2\pi}{\hbar}\sum_{\alpha_1,\alpha_2,\alpha_3,\alpha_4}|D-E|^2\,\delta(E_3-E_1+E_4-E_2) \quad (1)$$

and use P as a direct measure for the APS signal. In Eq. (1) E_i ($i=1,\ldots,4$) are the energies corresponding to the various involved single-particle states ψ_{α_i} with quantum numbers α_i, while D and E are Coulomb matrix elements given by

$$D=\int d^3r_1\int d^3r_2\,\psi^*_{\alpha_1}(\vec{r}_1)\,\psi^*_{\alpha_2}(\vec{r}_2)\frac{e^2}{|\vec{r}_1-\vec{r}_2|}\,\psi_{\alpha_3}(\vec{r}_1)\,\psi_{\alpha_4}(\vec{r}_2), \quad (2)$$

$$E=\int d^3r_1\int d^3r_2\,\psi^*_{\alpha_1}(\vec{r}_1)\,\psi^*_{\alpha_2}(\vec{r}_2)\frac{e^2}{|\vec{r}_1-\vec{r}_2|}\,\psi_{\alpha_4}(\vec{r}_1)\,\psi_{\alpha_3}(\vec{r}_2). \quad (3)$$

Here the quantum numbers α_1 and α_2 specify the initially occupied core and incoming low-energy electron diffraction

(LEED) states, respectively, including their spin character. The band states labeled by the quantum numbers α_3 and α_4, on the other hand, are initially unoccupied; i.e., their energies E_3 and E_4 lie above the Fermi energy. This energetic situation is sketched in Fig. 1 together with the so-called direct and exchange transitions represented by the matrix elements D and E, respectively.

In evaluating the matrix elements D and E as well as the sum over the substates distinguished by the quantum numbers α_i in Eq. (1), we closely follow the formalism developed by Hörmandinger *et al.* to deal with CCV and CVV AES.[21,19] Because APS can be viewed as an inverse CVV-AES experiment, it is obvious that the main difference to the investigations of these authors is that states taken to be occupied in the former case are unoccupied in the later and vice versa. In addition, the state ψ_{α_2} is a true LEED state and not a time-reversed LEED state as for AES. Furthermore, because we want to supply a description for the spin-resolved APS for spin-polarized systems, spin-selection rules for the matrix elements D and E will be taken explicitly into account, in contrast to the work of Hörmandinger *et al.*[21,19]

To calculate the transition probability P in Eq. (1) it is advantageous to split the square of the difference of D and E as

$$P=\frac{2\pi}{\hbar}\sum_{\alpha_1}\sum_{\alpha_2}\sum_{\alpha_3}\sum_{\alpha_4}[|D|^2+|E|^2-2\ \mathrm{Re}(D^*E)]\times\delta(E_3-E_1+E_4-E_2)[1-f(E_3)][1-f(E_4)], \quad (4)$$

with $f(E)$ the Fermi function. Using the explicit expression for D in Eq. (2) one gets for the first term

$$\begin{aligned}\overline{D(E_2)^2}&=\sum_{\alpha_1}\sum_{\alpha_2}\sum_{\alpha_3}\sum_{\alpha_4}|D|^2\delta(E_3-E_1+E_4-E_2)\\&=\sum_{\alpha_1}\sum_{\alpha_2}\sum_{\alpha_3}\sum_{\alpha_4}\int d^3r_1\int d^3r_2\int d^3r_1'\\&\quad\times\int d^3r_2'\psi_{\alpha_1}^*(\vec{r}_1)\psi_{\alpha_2}^*(\vec{r}_2)\frac{1}{|\vec{r}_1-\vec{r}_2|}\\&\quad\times\psi_{\alpha_3}(\vec{r}_1)\psi_{\alpha_4}(\vec{r}_2)\psi_{\alpha_1}(\vec{r}_1')\psi_{\alpha_2}(\vec{r}_2')\frac{1}{|\vec{r}_1'-\vec{r}_2'|}\\&\quad\times\psi_{\alpha_3}^*(\vec{r}_1')\psi_{\alpha_4}^*(\vec{r}_2')\delta(E_3-E_1+E_4-E_2). \quad (5)\end{aligned}$$

This expression can be simplified by twice making use of the identity

$$\sum_{\alpha}\psi_{\alpha}(\vec{r},E_{\alpha})\psi_{\alpha}^*(\vec{r}',E_{\alpha})\delta(E-E_{\alpha})=-\frac{1}{\pi}\sum_{\sigma}\mathrm{Im}G_{\sigma}(\vec{r},\vec{r}';E), \quad (6)$$

with $G_{\sigma}(\vec{r},\vec{r}';E)$ the spin-resolved single-particle Green's function. This quantity is a 2×2 matrix with respect to the spin indices. Because we ignore spin-orbit coupling and assume collinear spin magnetism, this matrix is diagonal. For the same reason, the states ψ_{α} have pure spin character and

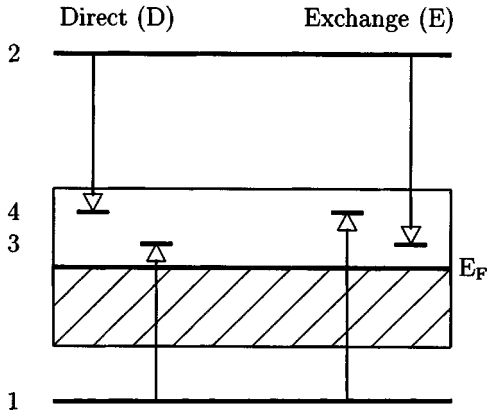

FIG. 1. One-electron excitation scheme for the APS. The arrows represent transitions corresponding to the direct (left) and exchange (right) matrix elements D and E, respectively. The labels 1 and 2 indicate the initially occupied core and incoming LEED states, respectively, while 3 and 4 are the finally occupied valence-band states above the Fermi level E_F.

the Green's function can be split unambiguously into two spin contributions G_{σ} that have nonzero elements only in the upper left or lower right corner, respectively [see Eqs. (8) and (9)]:

$$\begin{aligned}\overline{D(E_2)^2}&=\frac{1}{\pi^2}\sum_{\alpha_1}\sum_{\alpha_2}\sum_{\sigma_3}\sum_{\sigma_4}\int dE_4\int d\vec{r}_1\int d\vec{r}_2\\&\quad\times\int d\vec{r}_1'\int d\vec{r}_2'\psi_{\alpha_1}^*(\vec{r}_1)\psi_{\alpha_2}^*(\vec{r}_2)\frac{1}{|\vec{r}_1-\vec{r}_2|}\\&\quad\times\psi_{\alpha_1}(\vec{r}_1')\psi_{\alpha_2}(\vec{r}_2')\frac{1}{|\vec{r}_1'-\vec{r}_2'|}\mathrm{Im}G_{\sigma_3}(\vec{r}_1,\vec{r}_1';E_3)\\&\quad\times\mathrm{Im}G_{\sigma_4}(\vec{r}_2,\vec{r}_2';E_4), \quad (7)\end{aligned}$$

where E_3 is restricted by $E_3=E_2-E_4+E_1$. Using multiple scattering theory to represent the Green's functions one has[22]

$$\mathrm{Im}G_{\sigma}(\vec{r},\vec{r}';E)=\mathrm{Im}\sum_{L,L'}Z_{L\sigma}^i(\vec{r},E)\tau_{LL',\sigma}^{ii}Z_{L'\sigma}^i(\vec{r}',E)^{\dagger}. \quad (8)$$

Here it has been assumed that the spatial variables $\vec{r}$ and $\vec{r}'$ are restricted to the Wigner-Seitz cell at atomic site i. The functions $Z_{L\sigma}^i(\vec{r},E)$, with L standing for the set of quantum numbers (l,m_l), are solutions to the Schrödinger equation for the potential well at site i, which is assumed to be spherically symmetric. Adopting in addition the atomic sphere approximation by replacing the Wigner-Seitz cell by the Wigner-Seitz sphere, $Z_{L\sigma}^i(\vec{r},E)$ may be written as

$$Z_{L\sigma}^i(\vec{r},E)=Z_{l\sigma}^i(r,E)Y_L(\hat{r})\chi_{\sigma}, \quad (9)$$

with $Y_L(\hat{r})$ being a complex spherical harmonic and χ_{σ} a Pauli spinor. Here $Z_{l\sigma}^i(r,E)$ is normalized according to scattering theory;[22] i.e., it joins smoothly to $j_l t_l^{-1}-i\sqrt{E}h_l^+$ at the

Wigner-Seitz radius r_{WS}, with t_l the single-site t matrix and j_l and h_l^+ being the spherical Bessel and Hankel functions, respectively.[22]

The quantity $\tau^{ii}_{LL',\sigma}(E)$ in Eq. (8) is the so-called site-diagonal scattering path operator.[22] Because spin orbit was neglected, no spin cross terms occur; i.e., $\tau^{ii}_{LL',\sigma}$, as well as G_σ, is diagonal with respect to the spin index σ (see above). To simplify the resulting final expressions it will be assumed that $\tau^{ii}_{LL',\sigma}$ is also diagonal with respect to L. Furthermore, its dependence on m_l will be ignored. For cubic systems the former assumption is correct for $l \leqslant 2$, while the second one implies for the following that the difference in the density of states with t_{2g} and e_g character will be ignored; i.e., their average value will be used. These simplifications allow us to write

$$\mathrm{Im}\tau^{ii}_{LL',\sigma}(E) \approx -\frac{\pi}{2l+1} n^i_{l\sigma}(E) F^i_{l\sigma}(E)^{-1} \delta_{LL'}, \quad (10)$$

expressing $\mathrm{Im}\tau^{ii}_{LL',\sigma}$ in terms of the angular-momentum resolved density of states $n^i_{l\sigma}$ for the site i together with the corresponding overlap integral

$$F^i_{l\sigma}(E) = \int_0^{r_{\mathrm{WS}}} Z^i_{l\sigma}(r,E)^2 r^2 dr. \quad (11)$$

Having represented the final states ψ_{α_3} and ψ_{α_4} by means of the Green's function using multiple scattering theory, the initial states have to be expressed in a corresponding way. For the states ψ_{α_1} it is assumed that a complete core shell specified by the quantum number l_1 is involved. This means that in analogy to Eq. (9) one has

$$\sum_{\alpha_1} \psi_{\alpha_1}(\vec{r},E_1) = \sum_{m_{l_1}} \sum_{\sigma_1} R_{l_1\sigma_1}(r,E_1) Y_{L_1}(\hat{r}) \chi_{\sigma_1} \quad (12)$$

with the radial wave function $R_{l,\sigma}$ normalized to 1 within the Wigner-Seitz sphere.

Because APS is dealt with here in its spin-resolved mode, the incoming initial LEED state specified by the wave vector $\vec{k}$ will be taken to have pure spin character σ_2:

$$\sum_{\alpha_2} \psi_{\alpha_2}(\vec{r},E_2) = 4\pi \sum_{L_2} i^{l_2} t^i_{l_2}(E_2) \times Z^i_{l_2\sigma_2}(r,E_2) Y_{L_2}(\hat{r}) Y^*_{L_2}(\hat{k}) \chi_{\sigma_2}. \quad (13)$$

Here the single-scatterer approximation for ψ_{α_2} derived within multiple-scattering theory[23,24] has been used, which proved to be very reliable for the relevant energy range of E_2.[24] For the following it is convenient to replace $t_l Z_l$ in Eq. (13) by $e^{i\delta_{l\sigma}} \tilde{Z}_{l\sigma}$ with the phase shift $\delta_{l\sigma}$ related to the t matrix by $t_{l\sigma} = -1/\sqrt{E} \sin\delta_{l\sigma} e^{i\delta_{l\sigma}}$.

Making use of the identity

$$\frac{1}{|\vec{r}_1 - \vec{r}_2|} = \sum_{\lambda,\mu} \frac{4\pi}{2\lambda+1} \frac{r^\lambda_<}{r^{\lambda+1}_>} Y_{\lambda\mu}(\hat{r}_1) Y^*_{\lambda\mu}(\hat{r}_2), \quad (14)$$

the expression for $\overline{D(E_2)^2}$ as well as the corresponding ones for $\overline{E(E_2)^2}$ and $\overline{D^*E(E_2)}$ can be evaluated in a similar way as it has been done in the case of CVV AES by Hörmandinger *et al.*[19] This implies in particular that an integration over all directions $\hat{k}$ of the wave vector of the incoming LEED state electron is made[24] (this step is discussed in some detail in Sec. IV). This procedure leads to the expressions

$$\overline{D(E_2)}^2_{\sigma_2} = \int dE_4 \sum_{l_3,l_4,\sigma_3} n_{l_4\sigma_2}(E_4) n_{l_3\sigma_3}(E_3) \sum_{l_2,\lambda} \frac{(4\pi)^2}{2\lambda+1} \times (2l_1+1)(2l_2+1) \begin{pmatrix} l_4 & \lambda & l_2 \\ 0 & 0 & 0 \end{pmatrix}^2 \begin{pmatrix} l_1 & \lambda & l_3 \\ 0 & 0 & 0 \end{pmatrix}^2 \times [I^\lambda(R_{l_1\sigma_3} \tilde{Z}_{l_2\sigma_2} | R_{l_3\sigma_3} R_{l_4\sigma_2})]^2, \quad (15)$$

$$\overline{E(E_2)}^2_{\sigma_2} = \int dE_4 \sum_{l_3,l_4,\sigma_4} n_{l_4\sigma_4}(E_4) n_{l_3\sigma_2}(E_3) \sum_{l_2,\lambda} \frac{(4\pi)^2}{2\lambda+1} \times (2l_1+1)(2l_2+1) \begin{pmatrix} l_3 & \lambda & l_2 \\ 0 & 0 & 0 \end{pmatrix}^2 \begin{pmatrix} l_1 & \lambda & l_4 \\ 0 & 0 & 0 \end{pmatrix}^2 \times [I^\lambda(R_{l_1\sigma_4} \tilde{Z}_{l_2\sigma_2} | R_{l_4\sigma_4} R_{l_3\sigma_2})]^2, \quad (16)$$

$$\overline{D^*E(E_2)}_{\sigma_2} = \int dE_4 \sum_{l_3,l_4} n_{l_4\sigma_2}(E_4) n_{l_3\sigma_2}(E_3) \times \sum_{l_2,\lambda,\lambda'} (4\pi)^2 (2l_1+1)(2l_2+1) \times (-1)^{l_3+\lambda'+l_1} \begin{Bmatrix} l_3 & \lambda' & l_2 \\ l_4 & \lambda & l_1 \end{Bmatrix} \begin{pmatrix} l_1 & \lambda & l_3 \\ 0 & 0 & 0 \end{pmatrix} \times \begin{pmatrix} l_4 & \lambda & l_2 \\ 0 & 0 & 0 \end{pmatrix} I^\lambda(R_{l_1\sigma_2} \tilde{Z}_{l_2\sigma_2} | R_{l_3\sigma_2} R_{l_4\sigma_2}) \times \begin{pmatrix} l_1 & \lambda' & l_4 \\ 0 & 0 & 0 \end{pmatrix} \begin{pmatrix} l_3 & \lambda' & l_2 \\ 0 & 0 & 0 \end{pmatrix} \times I^{\lambda'}(R_{l_1\sigma_2} \tilde{Z}_{l_2\sigma_2} | R_{l_4\sigma_2} R_{l_3\sigma_2}). \quad (17)$$

Here use has been made of the spin selection rules $\delta_{\sigma_2\sigma_4}\delta_{\sigma_1\sigma_3}$ for D, $\delta_{\sigma_2\sigma_3}\delta_{\sigma_1\sigma_4}$ for E, and $\delta_{\sigma_1\sigma_2}\delta_{\sigma_3\sigma_4}\delta_{\sigma_1\sigma_3}$ for D^*E that become obvious from Fig. 1 and that arise because the interaction operator in Eq. (14) does not couple states with different spin character. However, one has to keep in mind that these spin selection rules still allow for spin mixing of D and E; i.e., the states 1 and 2 or, equivalently, 3 and 4 are allowed to have different spin character. Corresponding contributions to D and E will be denoted by $(\uparrow\downarrow)$ and $(\downarrow\uparrow)$ in the following. As it is also expected from Fig. 1, the expressions for $\overline{D(E_2)}^2_{\sigma_2}$ and $\overline{E(E_2)}^2_{\sigma_2}$ in Eqs. (15) and (16), respectively, are identical apart from the fact that the roles of states 3 and 4 are interchanged. Summation over all quantum numbers and integration with respect to E_4 together with the restriction $E_1+E_2=E_3+E_4$ leads to the identity $\overline{D(E_2)}^2_{\sigma_2} = \overline{E(E_2)}^2_{\sigma_2}$. Finally, the symbols

$$\begin{pmatrix} l_1 & l_2 & l_3 \\ m_1 & m_2 & m_3 \end{pmatrix}, \quad \begin{Bmatrix} l_1 & l_2 & l_3 \\ l_4 & l_5 & l_6 \end{Bmatrix}$$

are the usual $3j$ and $6j$ symbols[25] and the accompanying radial matrix elements $I^{\lambda}(f_1 f_2|f_3 f_4)$ are given by

$$I^{\lambda}(f_1 f_2|f_3 f_4)=\int r_1^2 dr_1 \int r_2^2 dr_2 f_1(r_1) f_2(r_2) \times \frac{r_<^{\lambda}}{r_>^{\lambda+1}} f_3(r_1) f_4(r_2). \tag{18}$$

The notation in Eqs. (15)–(17) indicates that the radial wave functions for the final band states have been normalized to 1; i.e., $R_{l_{3(4)}\sigma_{3(4)}}=Z_{l_{3(4)}\sigma_{3(4)}}/\sqrt{F_{l_{3(4)}\sigma_{3(4)}}}$.

Collecting all contributions to the transition probability, one may write the APS intensity in the compact form

$$P(E_2)_{\sigma}=\int_{E_a}^{E_b} dE \sum_{l,l',\sigma'} n_{l\sigma}(E) n_{l'\sigma'}(E') W_{l\sigma,l'\sigma'}(E,E'). \tag{19}$$

Here we introduced the cross section $W_{l\sigma,l'\sigma'}(E,E')$, which represents the sum of the various terms in Eqs. (15)–(17) and has the symmetric form

$$W_{l\sigma,l'\sigma'}(E,E')=W_{l'\sigma',l\sigma}(E',E). \tag{20}$$

This auxiliary quantity is given in explicit form by

$$W_{l\sigma,l'\sigma'}(E,E')=2S^{D}_{l\sigma,l'\sigma'}(E,E')+2\delta_{\sigma\sigma'}S^{DE}_{l\sigma,l'\sigma}(E,E'), \tag{21}$$

with

$$S^{D}_{l\sigma,l'\sigma'}(E,E')=(4\pi)^2(2l_1+1)\sum_{l_2,\lambda}\frac{2l_2+1}{2\lambda+1} \times [M^{l_2,\lambda}_{l\sigma,l'\sigma'}(E,E')]^2, \tag{22}$$

$$S^{DE}_{l\sigma,l'\sigma}(E,E')=(4\pi)^2(2l_1+1)\sum_{l_2,\lambda,\lambda'}(2l_2+1) \times(-1)^{l'+\lambda'+l_1}\begin{Bmatrix} l' & \lambda' & l_2 \\ l & \lambda & l_1 \end{Bmatrix} \times M^{l_2,\lambda}_{l\sigma,l'\sigma}(E,E')M^{l_2,\lambda'}_{l'\sigma,l\sigma}(E',E), \tag{23}$$

and the renormalized matrix elements

$$M^{l_2,\lambda}_{l\sigma,l'\sigma'}(E,E')=\begin{pmatrix} l & \lambda & l_2 \\ 0 & 0 & 0 \end{pmatrix}\begin{pmatrix} l_1 & \lambda & l' \\ 0 & 0 & 0 \end{pmatrix} \times I^{\lambda}(R_{l_1\sigma'}\tilde{Z}_{l_2\sigma}|R_{l'\sigma'}R_{l\sigma}). \tag{24}$$

This final expression for the APS signal intensity obviously means that P represents a sum over the folded angular-momentum-resolved density of states curves $n_{l\sigma}$ and $n_{l'\sigma'}$ weighted by the cross sections $W_{l\sigma,l'\sigma'}$. The range of energy for the folding of both curves is simply $E_a=E_F$ and $E_b=E_2+E_1-E_F$, with $E'=E_2-E+E_1$.

III. RESULTS AND DISCUSSION

A. Comparison with experiment

The formalism presented above has been implemented within a Korringa-Kohn-Rostoker band-structure program package and applied to calculate the spin-resolved APS spectra of bcc Fe and fcc Ni using Eqs. (15)–(19). Prior to a comparison of these raw spectra with experiment, however, a number of points have to be considered.

As a consequence of the transitions shown in Fig. 1, the core states ψ_{α_1} will be unoccupied and the process leading to a reoccupation of them can be used in experiment to monitor the APS process. Here one should note that this separation of the APS and the monitor processes is not rigorously justified. This also applies to the assumption that the APS intensity is independent of the detection mode, i.e., on whether the Auger or fluorescence process is used to monitor APS. In general, it is assumed that fluorescence detection gives the most direct measure for the rate of the central APS transition.[10] Indeed, the experimental data shown below have been obtained using this technique.[9]

Comparing theoretical spectra based on Eq. (19) with experiment one furthermore has to account for various lifetime and apparative broadening mechanisms. This is done in general by broadening the theoretical spectra by a Lorentzian of constant width Γ_c to account for the finite lifetime of the core hole. Finite lifetime effects due to the final band states are accounted for by using a Lorentzian with an energy-dependent width $\Gamma_v(E)$. Here we follow the suggestion of Ertl *et al.*,[9] assuming a linear increase of the width $\Gamma_v(E)=\gamma_v(E-E_F)$ with the distance from the Fermi energy. Apparative broadening is represented by folding the resulting spectra with a Gaussian line of width W.[9] The broadening parameters used here have been adjusted to some extent to optimize agreement with experiment starting with the values suggested by Ertl *et al.*[9] As discussed by these authors, it seems to be most appropriate to set Γ_c to zero. This led to the broadening parameters $\gamma_v=0.40\ \mathrm{eV}^{-1}$ and $W=0.5$ eV for Fe and $\gamma_v=0.15\ \mathrm{eV}^{-1}$ and $W=0.6$ eV for Ni, respectively. Finally, one has to mention that in experiment not $P(E_2)_{\sigma_2}$ itself is recorded, but, because the energy E_2 is modulated to improve the signal-to-noise ratio, the APS signal I is given by the corresponding energy derivative

$$I(E_2)_{\sigma}=\frac{d}{dE_2}\int_{E_F}^{E_2+E_1-E_F} dE \times \sum_{l,l',\sigma'} n_{l\sigma}(E) n_{l'\sigma'}(E') W_{l\sigma,l'\sigma'}(E,E'). \tag{25}$$

Figures 2 and 3 now show the integral and differential theoretical spin-resolved APS spectra of bcc Fe and fcc Ni obtained from Eqs. (19) and (25), respectively. The energy zero for these figures coincides with the onset of the unbroadened theoretical spectra; i.e., it corresponds to $E_2-E_F=E_F-E_1$ and $E_a=E_b=E_F$ in Eqs. (19) and (25). The experimental differential spectra that have been added in

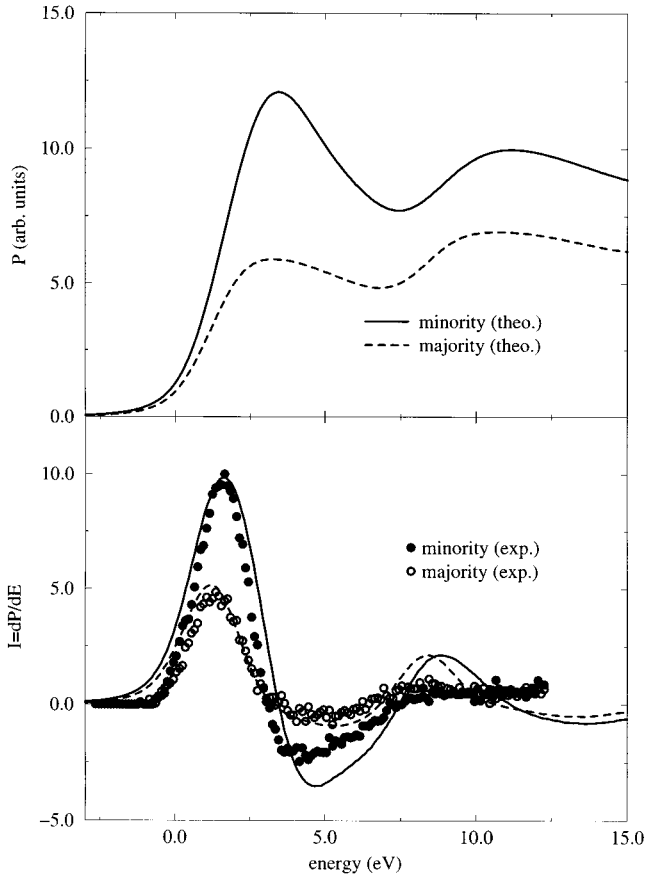

FIG. 2. Integral (top) and differential (bottom) spin-resolved APS spectra for bcc Fe, calculated using Eqs. (19) and (25). The differential experimental L_{III} spectra stem from Ertl *et al.* (Ref. 9).

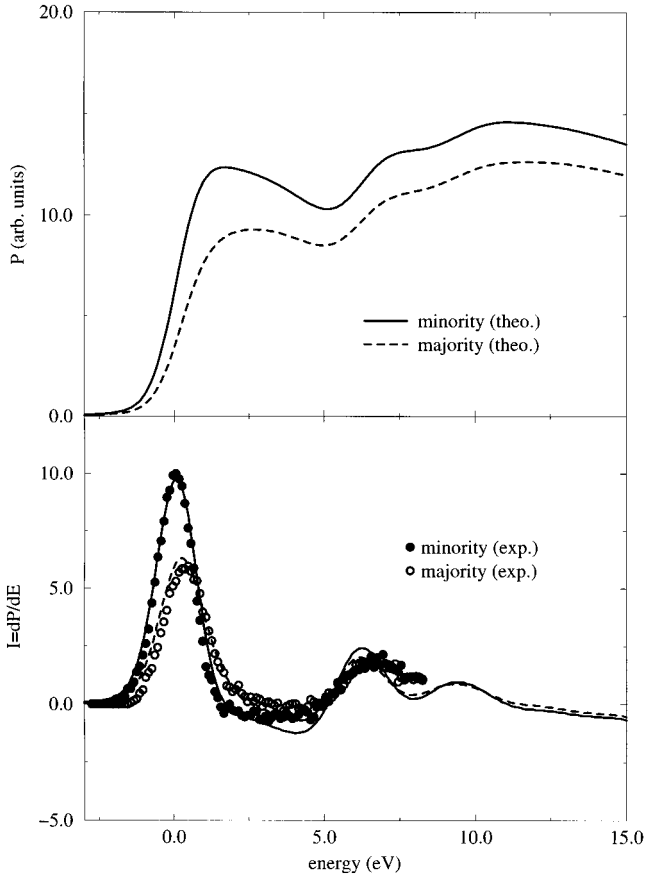

FIG. 3. Same as for Fig. 2, but for fcc Ni.

Figs. 2 and 3 were recorded using the L_{III} transition. This means that at energies higher than the displayed region the corresponding L_{II} spectra would follow, shifted by the spin-orbit splitting of the $2p$ core levels. For the comparison with the theoretical spectra, the experimental spectra have been aligned with the zero of energy corresponding to an energy of primary electrons of about 705 and 851 eV, respectively, on an absolute scale.

Comparing the various spin-resolved theoretical and experimental spectra with one another, rather satisfying agreement is found. This implies first of all that there are obviously no prominent correlation-induced features present in the experimental spectra. For that reason it is indeed justified to interpret the experimental APS spectra primarily as a measure for the cross-section-weighted self-convolution of the DOS above the Fermi energy for the systems investigated here. Because the energy-dependent radial matrix elements given in Eq. (18) vary quite smoothly with energy (see below), the prominent features of the experimental APS spectra can be directly linked to corresponding features of the DOS curve. Accordingly, the pronounced peaks at the onset of the Fe and Ni spectra can be ascribed directly to the high DOS around E_F for these elements together with the weighting step function $1-f(E)$ in Eq. (4). In line with this interpretation, the peaks at 8 and 6 eV in Figs. 2 and 3 have been ascribed, very similarly to the interpretation of x-ray-absorption spectra,[26] to critical points in the Brillouin zone that give rise to pronounced features in the DOS curves. In the case of Fe, the peak at 8 eV has been connected to the N_1 point,[27] while the L_7 point has been made responsible for the peak at 6 eV in the Ni spectrum.[28] While the bare DOS curves allow us to understand the main features of the APS spectra, they are not sufficient to explain finer details and in particular the relative intensities of the spin-resolved spectra. This has been demonstrated by Ertl *et al.*,[9] who used the bare spin- and angular-momentum-resolved DOS of Fe and Ni to simulate their spin-resolved APS spectra ignoring any cross sections. Only by introducing and fitting energy-independent weighting parameters meant to represent the cross sections could they achieve reasonable agreement with experiment. This means that the cross sections, calculated here in a parameter-free way, play a central role for the understanding of the spin-resolved APS spectra. This point will be analyzed in more detail in the following subsection.

B. Decomposition of the theoretical spectra

Calculation of integral and differential spin-resolved APS spectra via Eqs. (19) and (25), respectively, allows for an obvious decomposition of these spectra into their spin- and angular-momentum-resolved contributions. Corresponding curves are given in Figs. 4 and 5 for the differential spectra (only these will be discussed in the following because only these are normally recorded in experiment). As one would expect from the DOS of Fe and Ni, the contributions involving only d states are by far dominating. For the same reason,

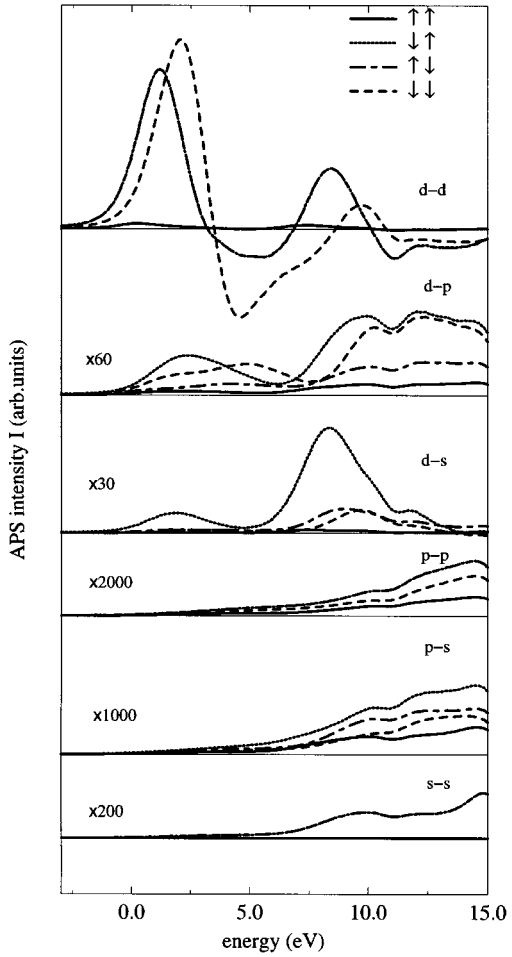

FIG. 4. Spin- and angular-momentum decomposition of the differential APS spectra $I(E_2)_{\sigma_2}$ of bcc Fe, according to Eq. (25).

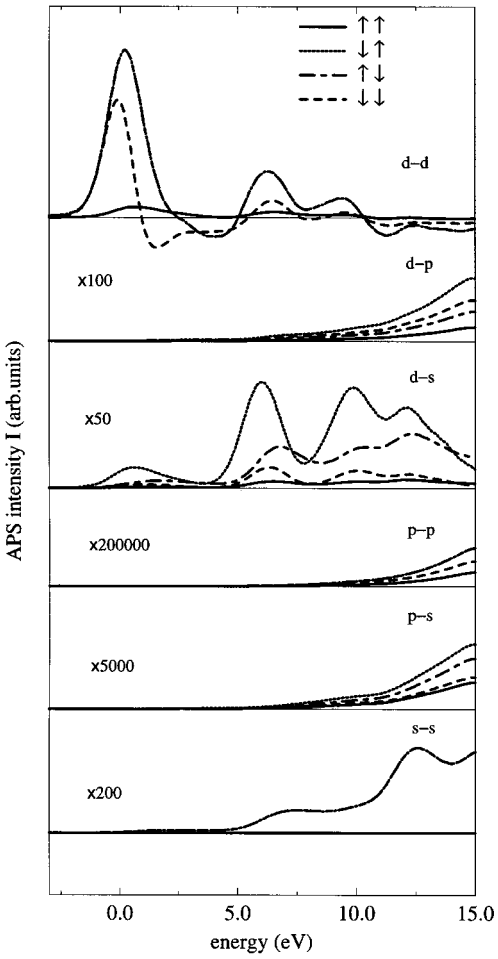

FIG. 5. Same as for Fig. 4, but for fcc Ni.

those involving minority d states ($d\downarrow$) are more important than those involving majority d states (d↑). This feature is slightly more pronounced for Ni than for Fe because Ni is a strong ferromagnet in the sense that its majority d band is more or less filled. Furthermore, one notes that contributions labeled with two opposite spin characters ($\uparrow\downarrow$) are of the same order of magnitude as those for two equal spin characters ($\uparrow\uparrow$ and $\downarrow\downarrow$). The reason for this is that the $\uparrow\downarrow$ contributions do not involve any spin-flip process (spin is a good quantum number; see above), but they merely lack the cross term $\overline{DE}$ in Eqs. (4) and (17). As one can see in Figs. 4 and 5, contributions involving s and p states are important only if these involve also d states, while pp, ps, and ss contributions are negligible.

The various partial spectra shown in Figs. 4 and 5 include the proper transition cross sections $W_{l\sigma,l'\sigma'}$ according to Eq. (21). To demonstrate the role of the weighting cross sections or matrix elements, respectively, some selected partial spectra of Fe are plotted in Fig. 6 together with spectra that have been derived from the DOS curves alone. For comparison, the later ones have been scaled by a constant factor to bring the two d↓d↓ spectra in coincidence as far as possible. Comparing both d↓d↓ spectra (with and without cross sections), one recognizes that there has to be a non-negligible energy dependence of the cross sections. This is found to be even more pronounced for the other partial spectra shown in Fig. 6. Here one has to note that the energy dependence of the cross sections stem only from the radial part I^{λ} given in Eq. (18). Because the core state energy E_1 is fixed and because of energy conservation, I^{λ} can be seen as a function of the energies E_2 and E_3 or E_2 and E_4. Alternatively, one can look upon the radial Coulomb matrix elements I^{λ} as a function of E_3 and E_4. Some selected corresponding cross sections $W_{l\sigma,l'\sigma'}(E,E')$ are plotted in Fig. 7. Here we show only cross sections for ↓↓-spin character because those for ↑↑ or ↓↑ character are very similar concerning their energy dependence and relative weight. As expected from the comparison in Fig. 6, one notes an appreciable dependence of the radial matrix elements on the energies E_3 and E_4. This is most pronounced for those involving d states. Here one even finds a maximum very similar to the finding for the $L_{2,3}$ x-ray absorption[26] or the spin-orbit coupling matrix elements. The reason for this behavior is the strong variation of the d wave function for the relevant range of energy because its character is gradually changing from $3d$ to $4d$, i.e., a radial node appears and migrates inward with increasing energy.

The comparison in Fig. 6 and the cross sections shown in Fig. 7 reveal not only the energy dependence of the matrix elements but also the different weight introduced by them for the various partial spectra. To quantify the later point, the

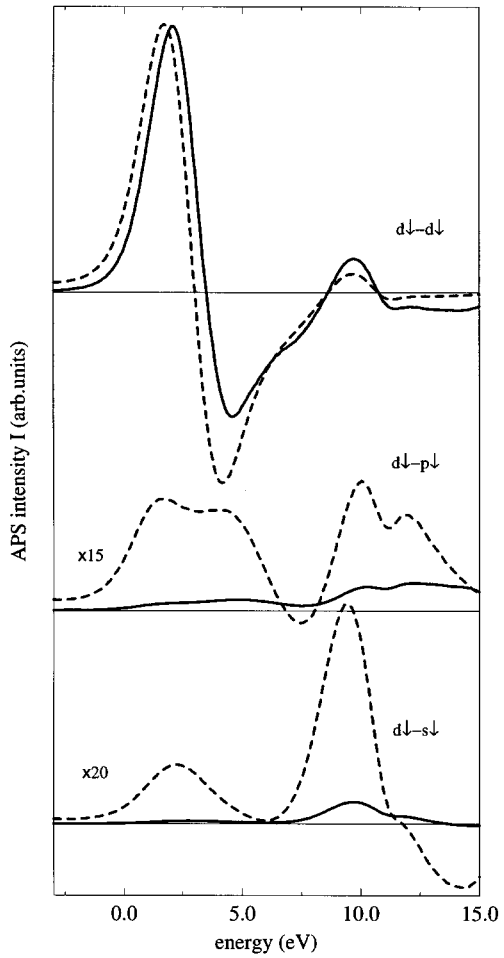

FIG. 6. Comparison of some selected spin- and angular-momentum decomposed differential APS spectra $I(E_2)_{\sigma_2}$ of bcc Fe calculated with (full lines) and without (dashed lines) the cross sections.

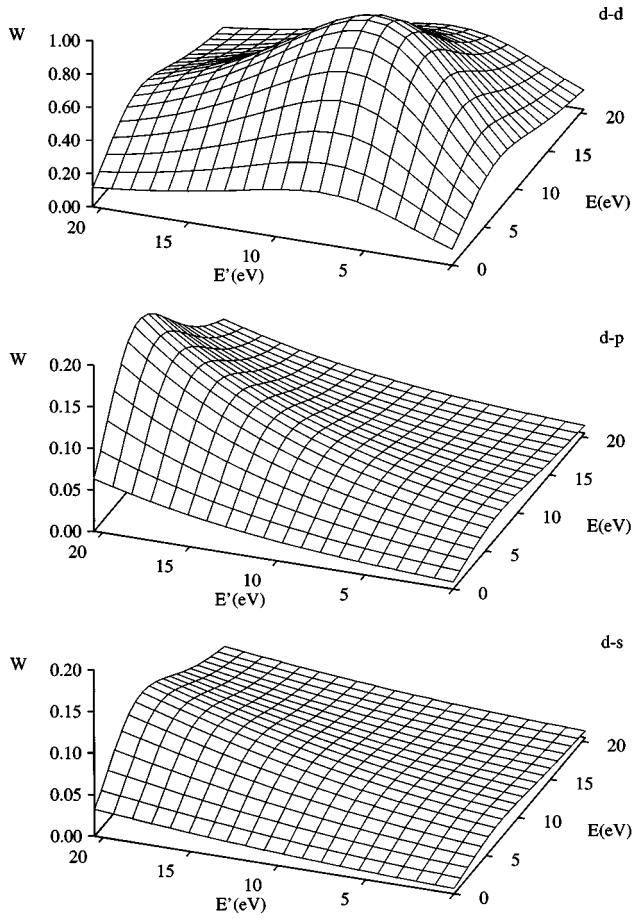

FIG. 7. Selected spin- and angular momentum resolved cross sections $W_{l\sigma,l'\sigma'}(E,E')$ [see Eq. (21)] for bcc Fe corresponding to Fig. 6, i.e., for $l=d$; $l'=s,p,d$; and $\sigma=\sigma'=\downarrow$. These functions have been scaled to have the maximum value of $W_{d\downarrow,d\downarrow}(E,E')$ at 1.

cross sections $W_{l\sigma,l'\sigma'}(E,E')$ as entering in Eqs. (19) and (25) are given in Table I for the most important transitions. Here the energies E and E' have been fixed to E_F; i.e., the data correspond to the onset of the spectra. As one can see, these cross sections once more favor transitions involving *d* states compared to those involving only *s* and *p* states. Here one should emphasize that in contrast to the radial Coulomb matrix elements I^{λ}, the cross sections $W_{l\sigma,l'\sigma'}$ collect all angular-momentum contributions together with the corresponding angular matrix elements according to Eqs. (15)–(17). As mentioned above, there is no very pronounced spin dependence for the cross sections to be seen. Comparing the data for Fe and for Ni, one notes that the relative weights of the various transitions are quite similar for both elements. This finding is in contrast with the results of Ertl *et al.*,[9] who fitted weight factors for the bare DOS-derived APS spectra to optimize agreement with experiment, obtaining a rather different distribution of the weights for Fe and Ni this way. Without doubt, the difference in the weights given in Table I is caused to some extent by the fact that the calculated cross sections $W_{l\sigma,l'\sigma'}(E,E')$ are energy dependent and listed here for $E=E'=E_F$, while the fitted weights are assumed to be energy independent and meant to represent $W_{l\sigma,l'\sigma'}(E,E')$ for the whole relevant range of energies. Nevertheless, one has to note that also the relative weights obtained from the fitting procedure differ quite strongly from the calculated ones. For this reason, one has to conclude that the fitting approach, while producing the main trend, should not be overstressed.

IV. CONCLUDING REMARKS

In the formalism presented in Sec. II the effect of the spin-orbit splitting of the core states has been ignored. If necessary, this restriction can straightforwardly be removed by dealing with these states in a fully relativistic way, accounting for the spin polarization at the same time.[29] After transforming the corresponding wave functions from the standard relativistic (κ,μ) representation (κ and μ are the spin orbit and magnetic quantum numbers, respectively) to the nonrelativistic (l,m_l,m_s) representation, the new wave functions can be used in the expressions given above. In addition, relativistic effects for the involved band states could be dealt with in a similar way as has been done for the CVV AES by Szunyogh *et al.*[30] However, according to experimental experience, not much impact of relativistic effects have to be expected for the systems investigated here. Finally, there seems to be no simple way to observe spin-orbit-

TABLE I. Calculated relative cross sections $W_{l\sigma,l'\sigma'}(E,E')$ for $E=E'=E_F$ normalized to $W_{d\uparrow,d\downarrow}(E_F,E_F)=1$ for bcc Fe and fcc Ni. The entry 0.0000 means that the value is smaller than 10^{-4}. For the unnormalized cross sections $W_{d\uparrow,d\downarrow}(E_F,E_F)_{\mathrm{Fe}}/W_{d\uparrow,d\downarrow}(E_F,E_F)_{\mathrm{Ni}}=1.2527$ was found. The values given in parentheses are the weights obtained by Ertl *et al.* by fitting the bare DOS-derived APS spectra to experiment. Those values not listed are fixed by Eq. (20).

$l\sigma,l'\sigma'$	Fe	Ni	$l\sigma,l'\sigma'$	Fe	Ni
$d\uparrow,d\uparrow$	0.2909 (0.00)	0.2145 (0.75)	$p\uparrow,p\uparrow$	0.0003 (0.80)	0.0000 (0.70)
$d\uparrow,d\downarrow$	1.0000 (1.00)	1.0000 (1.00)	$p\uparrow,p\downarrow$	0.0011 (0.10)	0.0000 (0.90)
$d\downarrow,d\uparrow$	1.0000 (1.00)	1.0000 (1.00)	$p\downarrow,p\uparrow$	0.0011 (0.10)	0.0000 (0.90)
$d\downarrow,d\downarrow$	0.1404 (0.18)	0.1909 (0.22)	$p\downarrow,p\downarrow$	0.0009 (0.80)	0.0000 (0.70)
$d\uparrow,p\uparrow$	0.0102 (0.00)	0.0000 (0.00)	$p\uparrow,s\uparrow$	0.0024 (0.00)	0.0000 (0.00)
$d\uparrow,p\downarrow$	0.0308 (0.28)	0.0000 (0.25)	$p\uparrow,s\downarrow$	0.0057 (0.00)	0.0000 (0.00)
$d\downarrow,p\uparrow$	0.0127 (0.28)	0.0000 (0.25)	$p\downarrow,s\uparrow$	0.0083 (0.00)	0.0000 (0.00)
$d\downarrow,p\downarrow$	0.0126 (0.00)	0.0000 (0.00)	$p\downarrow,s\downarrow$	0.0049 (0.00)	0.0000 (0.00)
$d\uparrow,s\uparrow$	0.0113 (0.00)	0.0034 (0.00)	$s\uparrow,s\uparrow$	0.0000 (0.00)	0.0000 (0.00)
$d\uparrow,s\downarrow$	0.0717 (0.00)	0.0173 (0.20)	$s\uparrow,s\downarrow$	0.0590 (0.00)	0.0091 (0.00)
$d\downarrow,s\uparrow$	0.0423 (0.00)	0.0191 (0.20)	$s\downarrow,s\uparrow$	0.0590 (0.00)	0.0091 (0.00)
$d\downarrow,s\downarrow$	0.0094 (0.00)	0.0034 (0.00)	$s\downarrow,s\downarrow$	0.0000 (0.00)	0.0000 (0.00)

induced magnetic dichroic phenomena[31] within spin-polarized APS using fluorescence detection.

In deriving the final expression for the APS signal intensity given in Eqs. (19) and (25) it was assumed that the corresponding experiment is essentially an angular-integrating one. This means that, in analogy to the corresponding description of AES,[21,19,30] an average has been taken with respect to the direction $\hat{k}$ of the incoming LEED electron [see Eq. (13)]. This is justified because for the experimental data shown here[9] $\hat{k}$ varies in a range 5–10°. Because of this, together with the high energy of the incoming electron of nearly 1 keV, the $\vec{k}$ selection rule for the partial transitions $2\rightarrow 4$ and $2\rightarrow 3$ in Fig. 1 is strongly relaxed. Therefore, it seems to be more appropriate to take the average with respect to $\hat{k}$ as it is done in general for valence-band x-ray photoemission spectroscopy.[24,32] Of course, it is straightforward to drop this averaging step to get a description for a true angular-resolved experiment performed at lower energies. This leads to expressions similar to those given in Eqs. (19) and (25); i.e., one still has a self-convolution of the DOS above E_F with the weighting cross section now being dependent on the direction $\vec{k}$ of the incoming electron.

The systems investigated here were treated as bulk systems, ignoring any influence of the surface. A first step to go beyond this approximation is to calculate the DOS entering Eqs. (19) and (25) in a layer-resolved way for the surface region. Summing the individual contributions of every layer weighted according to the mean-free-path length of the incoming LEED electron would account for the influence of the surface to a large extent. However, because the layer-resolved DOS rapidly approaches that of the bulk when going away from the surface (see, e.g., Refs. 33 and 34) not much difference can be expected for fcc Ni and bcc Fe compared to the present bulk results. On the other hand, the procedure sketched above seems to be an adequate approach to deal with surface layer systems, for example Fe on top of the (001) surface of fcc Cu that has been studied recently by Detzel *et al.*[11] for various thicknesses of the Fe top layer using spin-polarized APS in the fluorescence detection mode. Work along this line is in progress to provide a detailed theoretical description for these experiments.

V. SUMMARY

A theoretical description for spin-resolved APS has been presented that allows us to express the APS signal as a cross-section-weighted self-convolution of the DOS above the Fermi energy. The corresponding expression is quite general and, because of the element-specific nature of the central APS transition, it may be applied to pure as well as ordered and disordered many-component bulk systems. As has been demonstrated, dealing with surface layer systems in a proper way requires only some minor extensions. Finally, further refinement of the approach presented to account for the spin-orbit coupling of the involved core states as angular resolution in the corresponding experiment has been discussed.

Application of the present formalism to calculate spin-resolved APS spectra of bcc Fe and fcc Ni led to rather satisfying agreement with experiment. A decomposition of the theoretical spectra into their spin- and angular-momentum-resolved contributions reveal in detail the importance of the involved matrix elements or cross sections. As has been shown, these introduce some additional energy dependence for the various partial spectra and, more important, strongly influence their relative weight.

ACKNOWLEDGMENTS

The authors would like to thank M. Donath for many interesting and helpful discussions. Financial support by the German Ministry for Education and Research (BMBF) under Contract No. 05 621WMA 9, within the program *Zirkular Polarisierte Synchrotronstrahlung: Dichroismus, Magnetismus und Spinorientierung*, is also acknowledged.

[1] J. E. Houston and R. L. Park, J. Vac. Sci. Technol. **9**, 579 (1972).
[2] R. L. Park and J. E. Houston, J. Vac. Sci. Technol. **11**, 1 (1974).
[3] R. L. Park, Surf. Sci. **48**, 80 (1975).
[4] J. Kirschner, in *Electron Spectroscopy for Surface Analysis*, edited by H. Ibach, Topics in Current Physics Vol. 4 (Springer, Heidelberg, 1977).
[5] G. Ertl and J. Küppers, *Low Energy Electrons and Surface Chemistry* (Verlag-Chemie, Weinheim, 1985).
[6] S. Andersson and C. Nyberg, Surf. Sci. **52**, 489 (1975).
[7] T. Guo and M. L. den Boer, Phys. Rev. B **38**, 3711 (1988).
[8] J. Kirschner, Solid State Commun. **49**, 39 (1984).
[9] K. Ertl, M. Vonbank, V. Dose, and J. Noffke, Solid State Commun. **88**, 557 (1993).
[10] V. Dose, R. Drube, and A. Härtl, Solid State Commun. **57**, 273 (1986).
[11] T. Detzel, M. Vonbank, M. Donath, and V. Dose, J. Magn. Magn. Mater. **147**, L1 (1995).
[12] J. J. Lander, Phys. Rev. **91**, 1382 (1953).
[13] K. T. Schleicher, S. W. Schulz, R. Gmeiner, and H. U. Chun, J. Electron Spectrosc. Relat. Phenom. **31**, 33 (1983).
[14] S. W. Schulz, K. T. Schleicher, D. M. Rück, and H. U. Chun, J. Vac. Sci. Technol. A **2**, 822 (1984).
[15] W. Nolting, G. Geipel, and K. Ertl, Phys. Rev. B **44**, 12 197 (1991).
[16] W. Nolting, G. Geipel, and K. Ertl, Phys. Rev. B **45**, 5790 (1992).
[17] W. Nolting, G. Geipel, and K. Ertl, Z. Phys. B **92**, 75 (1993).
[18] M. Potthoff, J. Braun, G. Borstel, and W. Nolting, Phys. Rev. B **47**, 12 480 (1993).
[19] G. Hörmandinger, P. W. Weinberger, and J. Redinger, Phys. Rev. B **40**, 7989 (1989).
[20] D. Chattarji, *The Theory of Auger Transitions* (Academic Press, London, 1976).
[21] G. Hörmandinger, P. Weinberger, P. Marksteiner, and J. Redinger, Phys. Rev. B **38**, 1040 (1988).
[22] J. S. Faulkner and G. M. Stocks, Phys. Rev. B **21**, 3222 (1980).
[23] P. J. Durham, J. Phys. F **11**, 2475 (1981).
[24] H. Winter, P. J. Durham, and G. M. Stocks, J. Phys. F **14**, 1047 (1984).
[25] A. R. Edmonds, *Angular Momentum in Quantum Mechanics*, 2nd ed. (Princeton University Press, Princeton, 1960).
[26] H. Ebert *et al.*, Phys. Rev. B **53**, 16 067 (1996).
[27] A. Härtl, Ph.D. thesis, Bayerische Julius-Maximilians Universität Würzburg, 1985.
[28] V. Dose and G. Rensing, Solid State Commun. **48**, 683 (1983).
[29] H. Ebert, J. Phys.: Condens. Matter **1**, 9111 (1989).
[30] L. Szunyogh, P. Weinberger, and J. Redinger, Phys. Rev. B **46**, 2015 (1992).
[31] *Spin-Orbit Influenced Spectroscopies of Magnetic Solids*, edited by H. Ebert and G. Schütz, Lecture Notes in Physics Vol. 466 (Springer-Verlag, Heidelberg, 1996).
[32] T. Jarlborg and P. O. Nilson, J. Phys. C **12**, 265 (1979).
[33] S. Ohnishi, A. J. Freeman, and M. Weinert, Phys. Rev. B **28**, 6741 (1983).
[34] S. Ohnishi, C. L. Fu, and A. J. Freeman, J. Magn. Magn. Mater. **50**, 161 (1985).